Intracranial Gadolinium Deposition after Contrast-enhanced MR Imaging[1]

Robert J. McDonald, MD, PhD
Jennifer S. McDonald, PhD
David F. Kallmes, MD
Mark E. Jentoft, MD
David L. Murray, MD, PhD
Kent R. Thielen, MD
Eric E. Williamson, MD
Laurence J. Eckel, MD

Purpose: To determine if repeated intravenous exposures to gadolinium-based contrast agents (GBCAs) are associated with neuronal tissue deposition.

Materials and Methods: In this institutional review board–approved single-center study, signal intensities from T1-weighted magnetic resonance (MR) images and postmortem neuronal tissue samples from 13 patients who underwent at least four GBCA-enhanced brain MR examinations between 2000 and 2014 (contrast group) were compared with those from 10 patients who did not receive GBCA (control group). Antemortem consent was obtained from all study participants. Neuronal tissues from the dentate nuclei, pons, globus pallidus, and thalamus of these 23 deceased patients were harvested and analyzed with inductively coupled plasma mass spectrometry (ICP-MS), transmission electron microscopy, and light microscopy to quantify, localize, and assess the effects of gadolinium deposition. Associations between cumulative gadolinium dose, changes in T1-weighted MR signal intensity, and ICP-MS–derived tissue gadolinium concentrations were examined by using the Spearman rank correlation coefficient (ρ).

Results: Compared with neuronal tissues of control patients, all of which demonstrated undetectable levels of gadolinium, neuronal tissues of patients from the contrast group contained 0.1–58.8 μg gadolinium per gram of tissue, in a significant dose-dependent relationship that correlated with signal intensity changes on precontrast T1-weighted MR images (ρ = 0.49–0.93). All patients in the contrast group had relatively normal renal function at the time of MR examination. Gadolinium deposition in the capillary endothelium and neural interstitium was observed only in the contrast group.

Conclusion: Intravenous GBCA exposure is associated with neuronal tissue deposition in the setting of relatively normal renal function. Additional studies are needed to investigate the clinical significance of these findings and the generalizability to other GBCAs.

Online supplemental material is available for this article.

[1]From the Departments of Radiology (R.J.M., J.S.M., D.F.K., K.R.T., E.E.W., L.J.E.), Neurosurgery (D.F.K.), and Laboratory Medicine and Pathology (M.E.J., D.L.M.), College of Medicine, Mayo Clinic, 200 First St SW, Rochester, MN 55905. Received January 5, 2015; revision requested January 19; revision received January 28; accepted February 4; final version accepted February 12. **Address correspondence to** R.J.M. (e-mail: *mcdonald.robert@mayo.edu*).

Gadolinium-based contrast agents (GBCAs) represent a family of aminopolycarboxylic acid ligands chelated to gadolinium, a rare earth metal capable of altering the relaxivity of nearby water molecules by means of interaction with its unpaired electrons (1). When used in magnetic resonance (MR) imaging, this interaction expands the range of signal intensities detected during the examination and permits the detection of a wide variety of pathologic processes, including inflammation, infection, and malignancy, that would otherwise be undetectable with unenhanced MR imaging or other imaging modalities (2–4). Indeed, GBCAs have markedly expanded the diagnostic utility of MR imaging, with more than 10 million intravenous doses administered annually in the United States alone (4,5).

As free gadolinium is cytotoxic, the presence of the organic ligand serves as a physiologic chaperone, allowing an otherwise toxic metal to be safely administered intravenously and excreted (1,6–8). Despite relatively uncomplicated initial clinical trials in the early 1990s, a 2006 study causally associated the administration of gadolinium with the development of nephrogenic systemic fibrosis in patients with preexisting renal dysfunction (9). Subsequent studies implicated renal disease as the causative mechanism of gadolinium accumulation in the skin among patients with nephrogenic systemic fibrosis (10). These findings fueled concerns over the in vivo stability of GBCAs and their propensity toward transmetallation (gadolinium metal exchange for an endogenous cation). However, during the next several years nephrogenic systemic fibrosis was virtually eradicated through judicious use of GBCAs among patients with compromised renal function, increasing confidence in the safety of GBCA use in patients with preserved renal function (11–13).

Recently, indirect evidence has emerged that suggests gadolinium deposition may occur in patients with otherwise normal renal function. Several studies have demonstrated progressive increases in T1-weighted MR signal in various central nervous system (CNS) structures following repeated gadolinium administration (14,15). However, these signal intensity changes are nonspecific and can be seen with several other pathologic conditions. Follow-up studies verifying the presence of neuronal tissue deposition of gadolinium with use of direct tissue assays on human subjects have been absent from the literature.

In the current study, we sought to confirm these initial reports of CNS gadolinium deposition with direct assessment of gadolinium accumulation in neuronal tissues among deceased patients previously exposed to multiple doses of intravenous gadolinium.

Advances in Knowledge

- Elemental gadolinium accumulates in neuronal tissues after intravenous administration of gadolinium-based contrast agents (GBCAs), even in patients with normal renal and hepatobiliary function.
- Inductively coupled plasma mass spectrometry (ICP-MS) of autopsied brains exposed to GBCAs demonstrated a significant dose-dependent relationship in the amount of gadolinium deposited within neuronal tissues (ρ = 0.96–0.99, $P < .0001$); gadolinium deposition occurred in all sampled sites (globus pallidus, thalamus, dentate, pons) and was greatest in the dentate nucleus, with concentrations of 0.3–58.8 μg of gadolinium per gram of tissue.
- Transmission electron microscopy revealed the presence of a majority of gadolinium deposits in the endothelial walls, whereas a smaller fraction crossed an otherwise intact blood-brain barrier, with deposits in the neural interstitium.
- Changes in precontrast T1 signal in the dentate strongly correlate with the amount of tissue gadolinium assayed with ICP-MS (ρ = 0.93, $P < .0001$).

Implications for Patient Care

- Neuronal tissue deposition of gadolinium appears to be cumulative over a patient's lifetime and occurs in the absence of renal or hepatobiliary dysfunction.
- Neuronal tissue deposition appears to take place in all patients exposed to gadolinium and is detectable with as few as four lifetime doses of GBCA.
- The clinical significance of these findings is incompletely understood at this time.

Materials and Methods

Design and execution of this single-center retrospective study was subject to institutional review board oversight and Health Insurance Portability and Accountability Act guidelines on patient data integrity and privacy.

Study Design and Population

Deceased patients who underwent autopsy following antemortem consent

Published online before print
10.1148/radiol.15150025 **Content code:** NR

Radiology 2015; 000:1–11

Abbreviations:
CNS = central nervous system
eGFR = estimated glomerular filtration rate
GBCA = gadolinium-based contrast agent
ICP-MS = inductively coupled plasma mass spectrometry

Author contributions:
Guarantors of integrity of entire study, R.J.M., J.S.M., D.L.M.; study concepts/study design or data acquisition or data analysis/interpretation, all authors; manuscript drafting or manuscript revision for important intellectual content, all authors; manuscript final version approval, all authors; agrees to ensure any questions related to the work are appropriately resolved, all authors; literature research, R.J.M., D.F.K., L.J.E.; clinical studies, R.J.M., J.S.M., D.F.K., M.E.J., D.L.M., L.J.E.; experimental studies, R.J.M., M.E.J., D.L.M.; statistical analysis, R.J.M., J.S.M.; and manuscript editing, all authors

Conflicts of interest are listed at the end of this article.

and received at least one unenhanced (control group) or at least four GBCA-enhanced (contrast group) MR examinations of the brain between 2000 and 2014 were included in this study. Exclusion criteria included patients younger than 18 years, neoplastic involvement of the prescribed regions of interest in the CNS, clinical documentation or MR evidence of posttreatment and/or postradiation changes to the prescribed CNS regions, history of multiple sclerosis (16), history of metabolic disease, history of metal toxicity, history of previous intravenous or intra-articular gadolinium exposure (control group only), or patients lacking precontrast axial T1-weighted MR images. All clinical and procedural data were extracted from our institutional electronic medical record system by using relational database software (Data Discovery and Query Building; IBM, Armonk, New York) as described in Appendix E1 (online).

MR Imaging and GBCA Administration

All patients in this study underwent MR imaging of the brain, which included an unenhanced T1-weighted axial sequence of the entire brain. MR examinations were performed with one of 16 MR instruments dedicated to neuroradiologic imaging at our institution (eight 1.5-T GE instruments [GE Healthcare, Little Chalfont, England], three 3.0-T GE instruments, two 1.5-T Siemens instruments [Siemens Healthcare, Erlangen, Germany], and three 3.0-T Siemens instruments). Unenhanced axial T1-weighted images were obtained by using the following common imaging parameters: repetition time = 400–700 msec, echo time = 10–15 msec, 256 × 192 matrix, and 4-mm-thick sections. Gadolinium-enhanced MR imaging of the brain was performed with the intravenous agent gadodiamide (Omniscan, GE Healthcare) by using an institutional weight-based nomogram for a target bolus dose of 0.1 mmol/kg. Renal function was assessed before each MR examination to screen for chronic renal failure by using estimated glomerular filtration rate (eGFR) derived from serum creatinine results collected within 24 hours of MR imaging (17). According to institutional policy, gadolinium contrast material is administered only when appropriate for the imaging study and is withheld from any patient with stage 4 or 5 chronic kidney disease (eGFR < 30 mL/min/1.73 m^2) or in the setting of ongoing acute kidney injury on the basis of American College of Radiology guidelines for the prevention of nephrogenic systemic fibrosis (12).

MR Imaging Data Analysis

MR images and data were extracted and analyzed (R.J.M., with 4 years of experience) from our institutional radiology information server by using a proprietary imaging viewer (QREADS; Mayo Clinic, Rochester, Minn) (18). Unenhanced T1-weighted MR signal intensities were quantified from prescribed neuroanatomic regions of interest in the posterior fossa (dentate nucleus and pons) and basal ganglia (globus pallidus and pulvinar of the thalamus) as shown in Figure 1. Mean T1-weighted signal intensities were computed for user-defined regions of interest within each prescribed region and normalized against the signal intensity of cerebrospinal fluid to account for intra- and intersequence signal intensity differences, differences among MR units, and magnetic field inhomogeneity along the primary magnetic field axis (z-axis). For patients who underwent at least two MR examinations, changes in T1 signal intensities between the last and first examination in each of the four prescribed neuroanatomic locations were quantified as the percentage change in normalized T1 signal intensity.

Tissue Processing

All autopsies with brain sectioning were performed by one of three board-certified staff neuropathologists (including M.E.J.) with 8–35 years of experience. Whole-brain specimens were removed at autopsy, formalin fixed for approximately 10 days, sectioned into approximately 0.5-cm-thick slices, placed in 10% neutral buffered formalin, and archived in our institutional biospecimen repository. Tissue samples for this study were harvested from the posterior fossa (dentate nucleus and pons) and basal ganglia (globus pallidus and thalamus) of archived whole-brain specimens and placed in formalin solution for further analysis. All samples were harvested from areas unaffected by posttreatment and/or postradiation changes through careful visual inspection and correlation with T2-weighted fluid-attenuated inversion recovery signal intensity changes that are commonly associated with these findings. Distances between the tumor or postradiation change margin relative to the harvested tissue were measured from MR imaging data. Laterality was maintained between MR imaging signal intensity analysis and sites of tissue harvesting. In addition, hematoxylin-eosin–stained microscope slides of the dentate, harvested at the time of autopsy for diagnostic purposes, were retrieved from pathology archives and reviewed.

Mass Spectrometry

Elemental gadolinium quantification of acid hydrolyzed tissue samples was performed with inductively coupled plasma mass spectrometry (ICP-MS) in our institutional heavy metals laboratory (D.L.M., with 18 years of experience). Formalin-fixed brain tissues were desiccated at 90°C for 4–6 hours, weighed, digested with a concentrated nitric acid (Fisher Scientific, Hampton, NH) at 80°C for 20 minutes, and subsequently diluted with an aqueous 30 wt% hydrogen peroxide. Samples were then diluted with 1% nitric acid containing rhodium and terbium internal standards. Tissue gadolinium quantification of stable gadolinium isotopes ^{157}Ga and ^{160}Ga was performed by using an inductively coupled plasma mass spectrometer (ELAN DRC II; Perkin Elmer, Shelton, Conn). Results from tissue mass spectrometry were compared with standard curves generated from internal standards purchased from the European Commission Joint Research Center (Geel, Belgium) and the National Institute of Standards and Technology (Gaithersburg, Md). For gadolinium ions, the analytical range of this instrument has been shown to

Figure 1

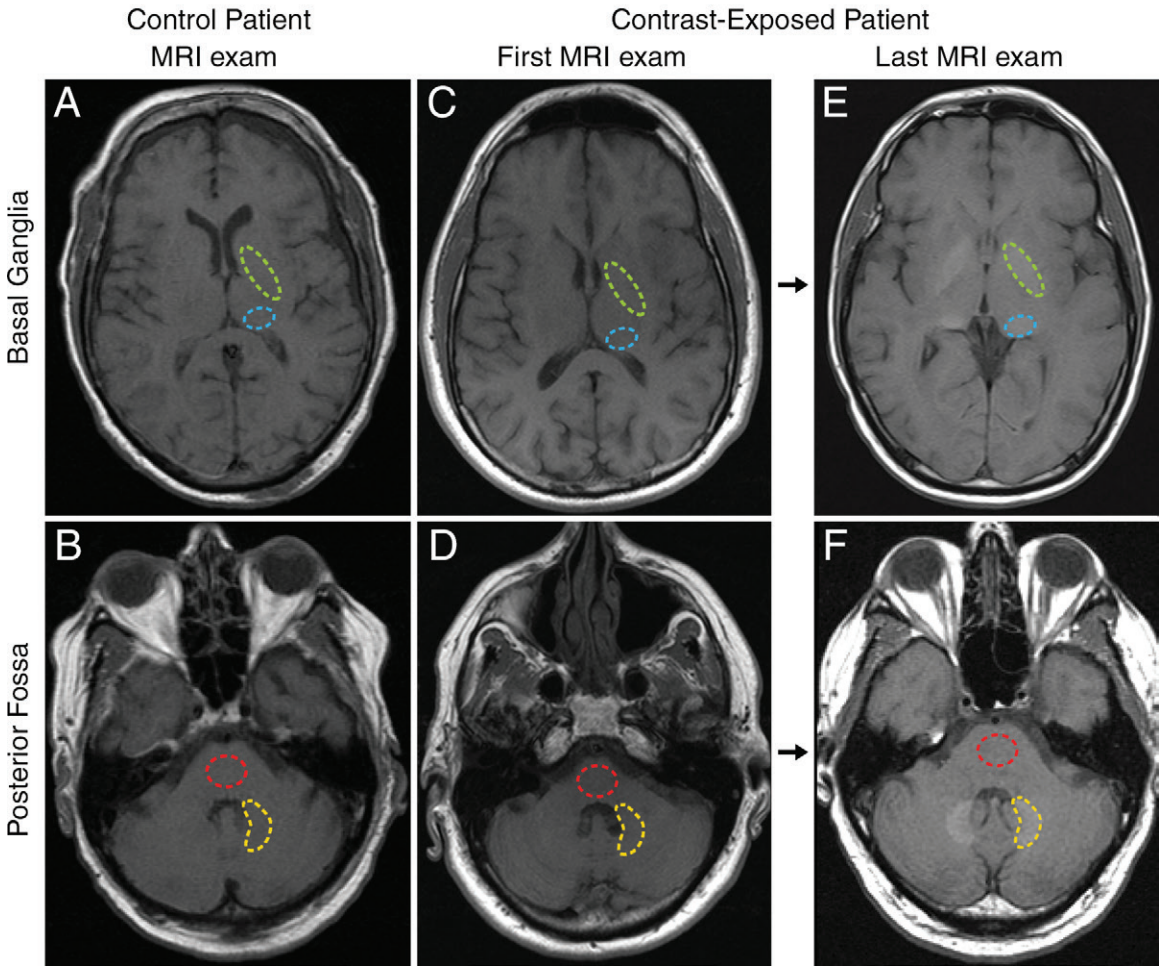

Figure 1: Axial T1-weighted MR images through, *A, C, E,* basal ganglia and, *B, D, F,* posterior fossa at level of dentate nucleus. Images are shown for, *A, B,* control group patient 4, and the, *C, D,* first and, *E, F,* last examinations performed in contrast group patient 13. Regions of interest used in quantification of signal intensity are shown as dashed lines for globus pallidus (green), thalamus (blue), dentate nucleus (yellow), and pons (red).

range from 0.1 to 1000 ng/mL. Tissue gadolinium concentration was determined by multiplying the weight of gadolinium per milliliter in the digested solution by the dilution factor and dividing by tissue sample weight.

Transmission Electron Microscopy with Electron Probe Microanalysis

Transmission electron microscopy was performed in conjunction with electron probe microanalysis at our institutional microscopy core facility (R.J.M., with 12 years of experience) to characterize and quantify the distribution of gadolinium deposits in these formalin-fixed tissues. Characteristic x-ray spectra formed during electron probe microanalysis permit highly accurate assessment of the elemental composition of structures identified with transmission electron microscopy. Formalin-fixed tissue samples were rinsed in 0.1 mol/L phosphate buffer, secondarily fixed in Trump fixative (4% paraformaldehyde + 1% glutaraldehyde in 0.1 mol/L phosphate buffer), dehydrated through an ethanol series, stained with 1% osmium tetroxide (wt/wt) and 1% uranyl acetate (wt/wt), and subsequently embedded in epoxy resin (Embed 812 + Araldite 502; EMS, Hatfield, Pa). Ultrathin embedded tissue sections (0.1 μm thick) were then stained with 2% lead citrate to enhance image contrast during microscopy. Additional ultrathin embedded sections were processed without the initial 1% osmium tetroxide (wt/wt) and 1% uranyl acetate (wt/wt) staining to better identify the presence of heavy metals within the section tissues. Stained samples were subsequently mounted on platinum grids. Micrographs were obtained by using a transmission electron microscope (Technai G^2 12; FEI, Hillsboro, Ore) equipped with an energy-dispersive spectrometry system (EDAX, Mahweh,

Table 1

Demographic and Clinical Characteristics of Study Population

Group and Patient No.	Age at Death (y)	Examination Indication*	No. of MR Examinations	Gadolinium Dose (mL)†	Interval between Imaging and Death (d)	eGFR (mL/min/1.73 m²)‡	Alkaline Phosphatase Level (U/L)‡§	Aspartate Aminotransferase Level (U/L)‡§	Total Bilirubin Level (mg/dL)‡§
Contrast group									
1	22	Encephalitis	4	52	18–84	94 (62–125)	86 (37–114)	29 (14–39)	0.4 (0.4–0.5)
2	50	CNS metastases	5	75	13–311	74 (59–89)	71 (53–80)	29 (17–49)	0.5 (0.4–1.2)
3	47	CNS metastases	6	85	86–520	54 (49–59)	57 (39–75)	42 (22–253)	0.4 (0.3–1.8)
4	62	GBM	7	129	29–338	78 (58–98)	84 (63–91)	18 (13–28)	0.7 (0.4–1.1)
5	46	CNS metastases	8	140	511–1610	108 (92–123)	83 (60–94)	25 (18–35)	0.5 (0.3–0.9)
6	72	Subependymoma	9	160	197–1266	103 (95–111)	78 (51–88)	28 (20–30)	0.5 (0.4–0.7)
7	51	GBM	10	162	44–427	81 (71–90)	60 (31–90)	22 (15–54)	0.6 (0.4–1.0)
8	61	CNS metastases	11	117	623–1169	88 (73–102)	85 (65–113)	34 (23–64)	0.6 (0.3–1.0)
9	60	GBM	11	199	20–403	96 (77–115)	158 (75–397)	50 (22–76)	1.1 (0.4–1.6)
10	69	Pituitary adenoma	14	241	17–3532	76 (67–84)	56 (38–81)	24 (17–39)	0.7 (0.6–0.8)
11	40	Oligodendroglioma	17	252	53–1059	105 (84–126)	51 (35–79)	26 (24–28)	0.5 (0.4–0.6)
12	61	GBM	28	500	62–983	83 (69–96)	58 (40–111)	27 (19–45)	0.6 (0.4–0.7)
13	40	GBM	29	420	106–2195	122 (95–149)	122 (106–131)	27 (18–106)	0.5 (0.4–0.6)
Control group									
1	84	TBI	1	…	3189	47 (47–47)	136 (78–298)	38 (27–86)	1.2 (0.5–2.0)
2	86	Dementia	2	…	3	62 (59–65)	190 (118–474)	60 (27–548)	0.5 (0.3–2.7)
3	62	Lymphoma	1	…	516	44 (41–49)	113 (95–155)	30 (19–85)	0.2 (0.1–0.2)
4	91	TIA	1	…	2	64 (51–72)	85 (71–544)	25 (14–62)	0.6 (0.5–3.0)
5	74	Dementia	1	…	791	40 (34–60)	66 (59–85)	18 (16–19)	0.7 (0.6–0.8)
6	56	Seizure	3	…	663	10 (8–11)	173 (109–457)	39 (20–87)	0.7 (0.3–1.2)
7	83	TIA	6	…	2032	62 (53–70)	103 (75–373)	41 (24–107)	0.7 (0.4–1.0)
8	92	Hydrocephalus	1	…	5008	43 (43–43)	150 (99–643)	21 (14–146)	0.6 (0.6–0.6)
9	89	Lymphoma	1	…	8	29 (18–37)	50 (38–72)	18 (18–18)	0.1 (0.1–0.1)
10	60	ICH	1	…	2359	104 (81–109)	62 (62–62)	32 (27–36)	0.7 (0.6–0.9)

* GBM = glioblastoma multiforme, ICH = intracranial hemorrhage, TBI = traumatic brain injury, TIA = transient ischemic attack.

† Cumulative gadolinium dose from all intravenous gadolinium-enhanced MR examinations. Gadodiamide concentration = 287 mg/mL.

‡ Data are medians, with range in parentheses.

§ Normal laboratory ranges for assays are as follows: alkaline phosphatase level, 45–142 U/L; aspartate aminotransferase level, 8–48 U/L; total bilirubin level, 0.1–1.0 mg/dL.

NJ). Image densitometry was performed with ImageJ (National Institutes of Health, Bethesda, Md) (R.J.M., with 12 years of experience) to quantify the fraction of electron-dense foci present within brain tissue interstitium relative to the total amount detected in the image (19).

Statistical Analysis

All statistical analyses were performed by R.J.M. and J.S.M. using software (R, version 3.1; R Foundation for Statistical Computing, Vienna, Austria) (20). Continuous variables were presented as medians and interquartile ranges owing to nonnormal data distributions unless otherwise noted. Differences in the amounts of gadolinium detected with ICP-MS in the four sampled neuronal tissues were assessed with the Mood median test.

Correlations between cumulative gadolinium dose, changes in T1-weighted signal intensities on MR images, the amount of gadolinium detected in neuronal tissues with ICP-MS, and other independent variables including age at the time of death, interval between gadolinium exposure and death, renal function, and hepatobiliary function were assessed by using the nonparametric Spearman rank correlation coefficient (ρ) for each neuroanatomic location. The relationships among the amount of gadolinium detected in neuronal tissues with ICP-MS, cumulative gadolinium dose, and the additional independent variables noted earlier were also assessed with a mixed multivariate model, with neuroanatomic location treated as a fixed effect and patient identifier as the random effect. Significance was assigned to differences of $P \leq .05$.

Results

Patient Population

Twenty-three deceased patients (13 in the contrast group; 10 in the control group) satisfied all inclusion and exclusion criteria for this study. The demographic and clinical characteristics of these patients are shown in Table 1. Most patients in the contrast group

underwent serial brain MR imaging for surveillance of known or resected CNS tumors. Nine of the 13 patients in the contrast group and eight of the 10 in the control group lived within Olmsted county, Minnesota, and received all of their adult health care at our medical center; the remaining four patients in the contrast group and two patients in the control group were regional patients within our extended health care network, permitting access to their outside medical records and prior radiologic examinations.

Patients within the contrast group underwent four to 29 contrast-enhanced MR examinations, whereas those in the control group underwent one to six unenhanced MR examinations. The median age at the time of death was significantly lower among patients in the contrast group when compared with the control group (51 years [range, 43–61.5 years] vs 83.5 years [range, 61.5–89.5 years], respectively; $P < .0001$). Similarly, the median age at the time of first MR examination was significantly lower for patients in the contrast group when compared with the control group (51 years [range, 42–61 years] vs 78.5 years [range, 58–87.5 years], respectively; $P < .0001$). The median interval between the last MR examination and death was significantly shorter in the contrast group than in the control group (53 days [range, 19–151.5 days] vs 727 days [range, 8–2359 days], respectively; $P < .0001$). Median baseline renal function during MR imaging was significantly higher in the contrast than in the control group (88 mL/min/1.73 m^2 [range, 77–104 mL/min/1.73 m^2] vs 45.5 mL/min/1.73 m^2 [range, 40–62 mL/min/1.73 m^2], respectively; $P < .0001$). Within the contrast group, the lowest recorded eGFR within 24 hours of gadolinium administration for MR imaging was 49 mL/min/1.73 m^2; most patients had eGFRs of at least 60 mL/min/1.73 m^2. Intravenous GBCA was never withheld from a patient in this group because of concern for acute or stage 4 or 5 chronic renal failure (eGFR < 30 mL/min/1.73 m^2). Median hepatobiliary function (alkaline phosphatase, aspartate aminotransferase, total bilirubin levels) was normal in most patients in the contrast group near the time of gadolinium administration (Table 1).

Ten of the 11 cases of intracranial malignancy in the contrast group were limited to the supratentorial region without posterior fossa involvement; patient 7 had multifocal glioblastoma multiforme with a small untreated lesion in the brachium pontis. All five treated patients diagnosed with glioblastoma multiforme underwent three-dimensional conformal radiation therapy as part of their standard treatment regimen; all treatments were performed on a supratentorial lesion. Two of the treated patients with CNS metastases (patients 3 and 8) underwent gamma knife therapy of a supratentorial lesion. With use of the periphery of peritumoral postradiation changes on MR images as a surrogate for the outer boundary of the low-dose conformal radiation field, all harvested samples from the supratentorial region (basal ganglia and thalamus) of radiation-exposed patients were at least 2 cm away from this boundary, with a median distance of 4 cm (range, 3–5 cm). Similarly, harvested samples from the posterior fossa were at least 6 cm away from this boundary, with a median distance of 8 cm (range, 7–9 cm). The remaining four cases of metastases, oligodendroglioma, and subependymoma (patients 2, 5, 6, and 11) did not undergo external beam radiation therapy; the median distance between these lesions and the sampled tissue sites in the supratentorial and posterior fossa regions were 5 cm (range, 4–6 cm) and 10 cm (range, 8–12 cm), respectively.

Effect of Gadolinium Exposure on Signal Intensity

Qualitative changes in T1-weighted signal intensity in the basal ganglia and posterior fossa after multiple administrations of gadolinium are shown in Figure 1; similar changes were not observed after successive unenhanced MR examinations (Fig E1 [online]). The association between cumulative gadolinium dose and normalized T1-weighted signal intensity changes in the basal ganglia and posterior fossa are shown in Figure 2, *A–D*. Whereas patients in the contrast group demonstrated a significant moderate to strongly positive dose–signal intensity correlation in all neuroanatomic locations ($\rho = 0.65–0.89$, $P < .02$), patients in the control group who underwent more than one unenhanced MR examination demonstrated no significant change in normalized T1-weighted signal intensity ($\rho = 0.09$, $P = .71$). The dentate nucleus was associated with the greatest dose-dependent change in T1-weighted signal intensity, whereas the pons demonstrated the lowest overall absolute change in T1-weighted signal intensity with gadolinium (Fig 2, *C* and *D*).

Effect of Gadolinium Exposure on Tissue Deposition

The effects of intravenous administration of a GBCA on the amount of gadolinium quantified in neuronal tissues with ICP-MS are shown in Table 2 and Figure 2, *E–H*. None of the patients in the control group had detectable levels of elemental gadolinium. In contradistinction, all patients exposed to multiple doses of a GBCA had elevated levels of elemental gadolinium in the four prescribed neuroanatomic regions, ranging from 0.1 to 58.8 μg gadolinium per gram of tissue (Table 2). Among all sampled neuroanatomic locations, the dentate nucleus contained the highest median concentrations of elemental gadolinium (Table 2; $\chi^2 = 13.6$, $P = .0035$). For each neuroanatomic location, cumulative gadolinium dose showed a very strong correlation with tissue gadolinium concentration (Fig 2, $\rho = 0.96–0.99$, $P < .0001$). Moderate to strong dose-dependent correlations were observed between T1-weighted signal intensity changes and tissue concentrations of gadolinium in all four neuroanatomic regions, ranging from $\rho = 0.49$ ($P = .08$) in the globus pallidus to $\rho = 0.89$ ($P < .0001$) in the dentate nucleus (Fig 2). Aside from cumulative gadolinium exposure, a weak association between median eGFR and tissue gadolinium concentration was identified ($\rho = 0.56$, $P = .05$) in the globus

Figure 2

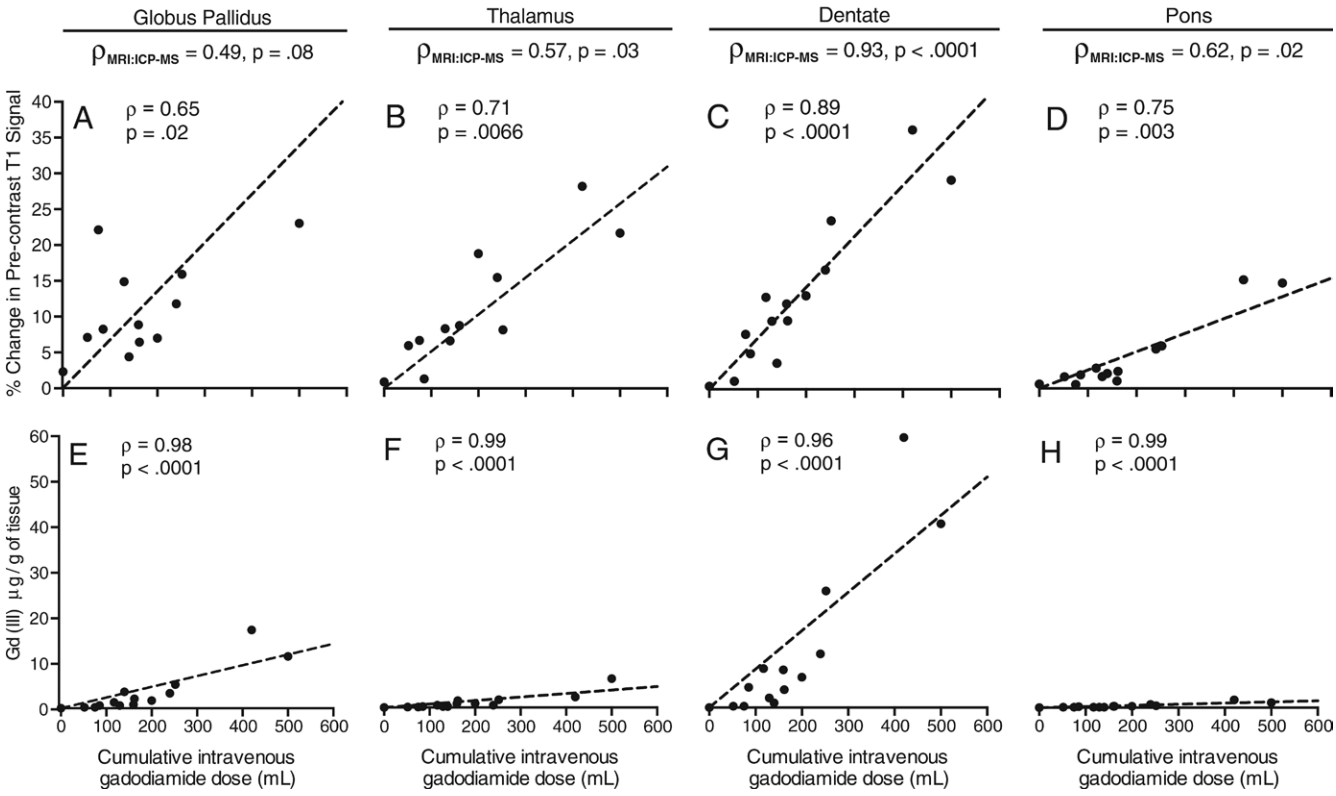

Figure 2: Gadolinium detection with mass spectrometry of cadaveric tissues and quantification of MR signal intensity changes. *A–D,* Changes in T1-weighted signal intensities in globus pallidus, thalamus, dentate, and pons are plotted against cumulative intravenous gadolinium exposure. *E–H,* Changes in gadolinium ion signal detected with mass spectrometry are plotted against cumulative intravenous gadolinium exposure. The strength of association between signal intensity changes and dose, gadolinium ion signal intensity and dose, and signal intensity changes and gadolinium ion signal intensity are shown with Spearman rank correlation coefficient (ρ) and associated *P* value.

pallidus; age at death, interval between last MR examination and death, and hepatobiliary function in all neuroanatomic locations and median eGFR in the remaining neuroanatomic locations all demonstrated nonsignificant correlations with tissue gadolinium concentration (Table E1 [online]). Multivariate analysis of these covariates revealed that cumulative gadolinium dose alone was significantly correlated with tissue gadolinium concentration when accounting for neuroanatomic location ($P < .0001$). Notwithstanding the weakly significant correlation between renal function and tissue gadolinium concentration, some of the highest tissue concentrations of gadolinium were present among patients with normal renal function (Tables 1 and 2).

Localization of Gadolinium within Neuronal Tissues and Assessment of Histologic Changes

Unlike control group patients, where gadolinium accumulation was not detected with transmission electron microscopy (Fig 3, *A*), x-ray microanalysis confirmed the presence of extensive gadolinium deposits within neuronal tissues of patients exposed to gadolinium (Fig 3, *B*). Among gadolinium-exposed samples, gadolinium was prominently clustered in large foci within the endothelial wall (Figs 3, *B,* and E2–E5 [online]); however, densitometry performed with wider field views suggested that 18%–42% of gadolinium appears to have crossed the blood-brain barrier and been deposited into the neural tissue interstitium (Figs E2–E5 [online]). Despite direct evidence of gadolinium deposition within neuronal tissues, we were unable to detect gross histologic changes between contrast and control groups in hematoxylin-eosin–stained tissues samples with visual light microscopy (Fig 3, *C* and *D*).

Discussion

The results of this single-center retrospective study demonstrate a significant dose-dependent relationship between intravenous GBCA administration and subsequent neuronal tissue deposition that was independent of patient age, sex, baseline renal function, or interval between gadolinium exposure and death. Despite the absence of obvious gadolinium-mediated histologic

Table 2

Results of Mass Spectrometry

Group and Patient No.	Dentate	Pons	Globus Pallidus	Thalamus
Contrast group				
1	0.1	0.2	0.0	0.0
2	4.4	0.2	0.6	0.2
3	0.3	0.1	0.2	0.1
4	2.1	0.1	0.6	0.2
5	1	0.1	3.6	0.2
6	8.2	0.3	0.8	0.8
7	3.9	0.3	2.1	1.5
8	8.5	0.1	1.3	0.5
9	6.6	0.3	1.7	0.9
10	11.7	0.7	3.3	0.5
11	25.4	0.4	5.2	1.7
12	40	1.1	11.4	6.3
13	58.8	1.7	17.2	2.3
Median	6.6 (1.55–18.55)	0.3 (0.1–0.55)	1.7 (0.6–4.4)	0.5 (0.2–1.6)
Control group				
1	0	0	0	0
2	0	0	0	0
3	0	0	0	0
4	0	0	0	0
5	0	0	0	0
6	0	0	0	0
7	0	0	0	0
8	0	0	0	0
9	0	0	0	0
10	0	0	0	0
Median	0 (0–0)	0 (0–0)	0 (0–0)	0 (0–0)

Note.—Data are tissue gadolinium concentrations detected with ICP-MS (in micrograms of gadolinium per gram of tissue). Numbers in parentheses are the interquartile range.

changes, we were able to directly detect gadolinium deposition in the interstitium of the neural tissues by using electron microscopy. Given the widespread use of GBCAs, our confirmation of gadolinium within neuronal tissues, even in the setting of normal renal and hepatobiliary function, merits additional investigation.

Our findings complement the observation of MR imaging signal intensity changes in the posterior fossa and basal ganglia by Errante et al (14) and Kanda et al (15). Similar to Errante et al (14), we were able to isolate our findings to a single linear ionic agent, gadodiamide, to better examine the effects of a single agent on changes in signal intensity; signal intensity changes in the study by Kanda et al (15) reflected patients who received a combination of gadopentetate dimeglumine and gadodiamide. In addition, our findings complement those of Errante et al (14) by demonstrating that these signal intensity changes take place in the absence of severe renal and hepatobiliary dysfunction (21–24).

Our findings expand on these preliminary efforts and now provide direct evidence of gadolinium tissue deposition with use of mass spectrometry and electron microscopy. Our data show that the T1-weighted signal intensity changes with MR imaging are highly correlated with tissue deposition. By using control patients, who were absent from the study by Errante et al (14), our findings suggest that the signal intensity changes observed with MR imaging are specific to gadolinium deposition. Furthermore, our gadolinium-exposed patient population underwent imaging almost exclusively for neoplastic processes, whereas previous studies included a combination of neoplastic, inflammatory, demyelinating, and degenerative processes. Because we excluded cases in which neoplasm and/or radiation therapy involved the basal ganglia or posterior fossa, our results are highly suggestive that this accumulation is occurring in nondiseased neuronal tissues. Finally, our data show that gadolinium accumulation is widespread throughout all sampled regions of the brain, suggesting that the MR signal intensity normalization methods used by Kanda et al (15) and Errante et al (14) should be modified in future studies.

Preclinical animal and human studies of gadodiamide and other GBCAs have long suggested pharmacokinetic behavior consistent with an extracellular distribution, with 90%–99% being cleared by means of renal excretion within 72 hours of administration and the remaining fraction being excreted into the bile by means of hepatic clearance (6,8,25,26). Our findings suggest a more complex pharmacokinetic behavior after intravenous administration. This observation is supported by data from White et al (27) and Darrah et al (28), who demonstrated that gadolinium is sequestered in bone matrix after intravenous administration. It remains possible that bone matrix may rapidly take up a small fraction of intravenously administered GBCA and act as a reservoir, slowly releasing gadolinium with subsequent uptake in other tissues.

In addition, the presence of gadolinium accumulation within nondiseased neuronal tissues in the presence of an apparently intact blood-brain barrier challenges our understanding of the biodistribution of GBCAs after intravenous administration (6,8,11,29). Although most of our patients exposed to gadolinium had primary or secondary brain malignancies, the regions of tumor involvement and postradiation changes were located in areas distant from the prescribed neuroanatomic locations. In contradistinction to

Figure 3

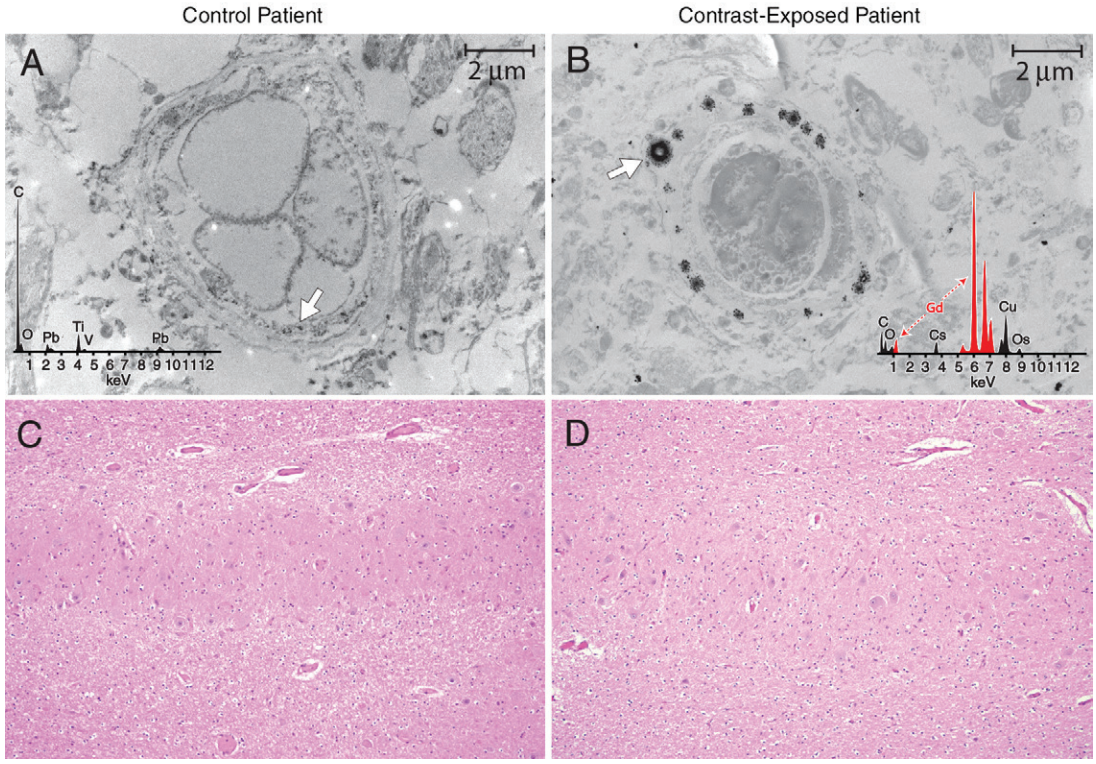

Figure 3: Tissue localization and cellular response to gadolinium deposition. *A, B*, Transmission electron micrographs (0.2% lead citrate stain; original magnification, ×10 000) of dentate nuclei tissue samples of, *A*, control patient 4 and, *B*, contrast group patient 13. X-ray spectra are also shown for selected electron-dense foci (arrow); gadolinium peaks in spectra are indicated by red overlay. *C* = carbon, *Cs* = cesium, *Cu* = copper, *Gd* = gadolinium, *O* = oxygen, *Os* = osmium, *Pb* = lead, *Ti* = titanium, *V* = vanadium. *C, D*, Photomicrographs from light microscopy (hematoxylin-eosin stain; original magnification, ×100) of dentate nuclei from, *C*, control patient 4 and, *D*, contrast group patient 13.

bone and other tissues, where gadolinium deposition can be explained by the presence of fenestrated capillary systems, our findings suggest that gadolinium from administered GBCA is able to cross an otherwise intact blood-brain barrier and that compromise of this barrier is not necessary for tissue deposition. The presence of numerous punctate foci of gadolinium in the endothelium of neuronal capillaries suggests that the blood-brain barrier is largely intact; however, because the distribution of this deposition within these tissues is not uniform, these foci may suggest a reactive cellular response to this metal. Reports of similar MR signal intensity changes in the dentate and/or deep gray nuclei among patients with multiple sclerosis, neurofibromatosis, hypoparathyroidism, inherited metabolic disorders, and Fahr disease may suggest that these areas are uniquely susceptible to metal deposition (14,15,30). However, the mechanisms of gadolinium sequestration, deposition, and nonuniform uptake in certain neuroanatomic locations remain poorly understood.

Additional questions and study limitations persist. First, it remains unclear if the gadolinium detected in neuronal tissues remains in a chelated state or free ionic form. Currently available tissue-based assays are only capable of detecting elemental gadolinium owing to technical limitations, as the extraction method and ionization of these tissues is destructive to the organic ligand (6,11). Speciation of gadolinium chelates is possible with use of serum-based assays, but these are of limited value in discerning the chelation state of tissue deposits—particularly in formalin-fixed tissue samples (31). Notwithstanding these limitations, future efforts directed toward discerning the chelation state of these gadolinium deposits will be crucial to our understanding of the mechanism of and risks associated with tissue deposition. Second, estimates of the relative amounts of gadolinium in the neural tissue interstitium should not be viewed as an exact quantitative assay of the amount of intracellular gadolinium that has crossed the blood-brain barrier. Third, although no clinical phenotype appears to be associated with our patient cohort, the expected physiologic effects and clinical significance of lanthanide metal deposition within neuronal

tissues is unknown and merits additional investigation. Fourth, although we were unable to identify an association between renal function and gadolinium accumulation, the small sample size of this study could mask weaker correlations. Finally, it remains unclear whether this deposition effect is limited to gadodiamide, to linear chelated GBCAs in general, or whether it manifests in both linear and the more thermodynamically stable macrocyclic gadolinium chelates; recent indirect evidence from Kanda et al (32) suggest this deposition may be limited to linear agents. Although our findings are limited to a single linear ionic GBCA (gadodiamide), established data on the chemical and biophysical properties of GBCAs suggest that this deposition is likely to occur with multiple agents and that the extent of this deposition likely correlates with the thermodynamic stability of these chelates (33).

In conclusion, our findings suggest that intravenous administration of GBCA is associated with dose-dependent deposition in neuronal tissues that is unrelated to renal function, age, or interval between exposure and death. Although we were unable to clearly identify a histologic phenotype of gadolinium deposition within neuronal tissues, our findings strongly argue for future research to assess the in vivo stability and safety of GBCAs.

Acknowledgments: The authors thank Amy Bluhm, BS, Trace Christensen, BS, Jon Charlesworth, BS, and Jeffery Salisbury, PhD, for their technical expertise.

Disclosures of Conflicts of Interest: R.J.M. disclosed no relevant relationships. **J.S.M.** Activities related to the present article: disclosed no relevant relationships. Activities not related to the present article: institution received a grant from GE Healthcare. Other relationships: disclosed no relevant relationships. **D.F.K.** Activities related to the present article: disclosed no relevant relationships. Activities not related to the present article: receives personal fees from GE Healthcare for serving on an advisory board. Other relationships: disclosed no relevant relationships. **M.E.J.** disclosed no relevant relationships. **D.L.M.** disclosed no relevant relationships. **K.R.T.** disclosed no relevant relationships. **E.E.W.** disclosed no relevant relationships. **L.J.E.** disclosed no relevant relationships.

References

1. Hao D, Ai T, Goerner F, Hu X, Runge VM, Tweedle M. MRI contrast agents: basic chemistry and safety. J Magn Reson Imaging 2012;36(5):1060–1071.
2. Edelman RR, Warach S. Magnetic resonance imaging (2). N Engl J Med 1993;328(11):785–791.
3. Edelman RR, Warach S. Magnetic resonance imaging (1). N Engl J Med 1993;328(10):708–716.
4. Zhou Z, Lu ZR. Gadolinium-based contrast agents for magnetic resonance cancer imaging. Wiley Interdiscip Rev Nanomed Nanobiotechnol 2013;5(1):1–18.
5. Caravan P, Ellison JJ, McMurry TJ, Lauffer RB. Gadolinium(III) chelates as MRI contrast agents: structure, dynamics, and applications. Chem Rev 1999;99(9):2293–2352.
6. Aime S, Caravan P. Biodistribution of gadolinium-based contrast agents, including gadolinium deposition. J Magn Reson Imaging 2009;30(6):1259–1267.
7. Cacheris WP, Quay SC, Rocklage SM. The relationship between thermodynamics and the toxicity of gadolinium complexes. Magn Reson Imaging 1990;8(4):467–481.
8. Oksendal AN, Hals PA. Biodistribution and toxicity of MR imaging contrast media. J Magn Reson Imaging 1993;3(1):157–165.
9. Grobner T. Gadolinium—a specific trigger for the development of nephrogenic fibrosing dermopathy and nephrogenic systemic fibrosis? Nephrol Dial Transplant 2006;21(4):1104–1108.
10. High WA, Ayers RA, Chandler J, Zito G, Cowper SE. Gadolinium is detectable within the tissue of patients with nephrogenic systemic fibrosis. J Am Acad Dermatol 2007;56(1):21–26.
11. Amet S, Launay-Vacher V, Clément O, et al. Incidence of nephrogenic systemic fibrosis in patients undergoing dialysis after contrast-enhanced magnetic resonance imaging with gadolinium-based contrast agents: the Prospective Fibrose Nephrogénique Systémique study. Invest Radiol 2014;49(2):109–115.
12. American College of Radiology Committee on Drugs and Contrast Media. ACR manual on contrast media. 9th ed. Reston, Va: American College of Radiology, 2013.
13. Moreau JF, Droz D, Sabto J, et al. Osmotic nephrosis induced by water-soluble triiodinated contrast media in man: a retrospective study of 47 cases. Radiology 1975;115(2):329–336.
14. Errante Y, Cirimele V, Mallio CA, Di Lazzaro V, Zobel BB, Quattrocchi CC. Progressive increase of T1 signal intensity of the dentate nucleus on unenhanced magnetic resonance images is associated with cumulative doses of intravenously administered gadodiamide in patients with normal renal function, suggesting dechelation. Invest Radiol 2014;49(10):685–690.
15. Kanda T, Ishii K, Kawaguchi H, Kitajima K, Takenaka D. High signal intensity in the dentate nucleus and globus pallidus on unenhanced T1-weighted MR images: relationship with increasing cumulative dose of a gadolinium-based contrast material. Radiology 2014;270(3):834–841.
16. Roccatagliata L, Vuolo L, Bonzano L, Pichiecchio A, Mancardi GL. Multiple sclerosis: hyperintense dentate nucleus on unenhanced T1-weighted MR images is associated with the secondary progressive subtype. Radiology 2009;251(2):503–510.
17. Levey AS, Bosch JP, Lewis JB, Greene T, Rogers N, Roth D. A more accurate method to estimate glomerular filtration rate from serum creatinine: a new prediction equation. Modification of Diet in Renal Disease Study Group. Ann Intern Med 1999;130(6):461–470.
18. Erickson BJ, Ryan WJ, Gehring DG. Functional requirements of a desktop clinical image display application. J Digit Imaging 2001;14(2 Suppl 1):149–152.
19. Rasband WS. ImageJ. Bethesda, Md: U.S. National Institutes of Health, 1997–2014.
20. R Development Core Team. R: A language and environment for statistical computing. Vienna, Austria: R Foundation for Statistical Computing, 2012.
21. Kaplan GD, Aisen AM, Aravapalli SR. Preliminary clinical trial of gadodiamide injection: a new nonionic gadolinium contrast agent for MR imaging. J Magn Reson Imaging 1991;1(1):57–62.
22. VanWagoner M, O'Toole M, Worah D, Leese PT, Quay SC. A phase I clinical trial with gadodiamide injection, a nonionic magnetic resonance imaging enhancement agent. Invest Radiol 1991;26(11):980–986.
23. Harpur ES, Worah D, Hals PA, Holtz E, Furuhama K, Nomura H. Preclinical safety assessment and pharmacokinetics of gadodiamide injection, a new magnetic resonance imaging contrast agent. Invest Radiol 1993;28(Suppl 1):S28–S43.
24. Van Wagoner M, Worah D. Gadodiamide injection: first human experience with the nonionic magnetic resonance imaging enhance-

ment agent. Invest Radiol 1993;28(Suppl 1): S44–S48.

25. Brasch RC, Weinmann HJ, Wesbey GE. Contrast-enhanced NMR imaging: animal studies using gadolinium-DTPA complex. AJR Am J Roentgenol 1984;142(3):625–630.

26. Weinmann HJ, Laniado M, Mützel W. Pharmacokinetics of GdDTPA/dimeglumine after intravenous injection into healthy volunteers. Physiol Chem Phys Med NMR 1984;16(2):167–172.

27. White GW, Gibby WA, Tweedle MF. Comparison of Gd(DTPA-BMA) (Omniscan) versus Gd(HP-DO3A) (ProHance) relative to gadolinium retention in human bone tissue by inductively coupled plasma mass spectroscopy. Invest Radiol 2006;41(3):272–278.

28. Darrah TH, Prutsman-Pfeiffer JJ, Poreda RJ, Ellen Campbell M, Hauschka PV, Hannigan RE. Incorporation of excess gadolinium into human bone from medical contrast agents. Metallomics 2009;1(6):479–488.

29. Pietsch H, Raschke M, Ellinger-Ziegelbauer H, et al. The role of residual gadolinium in the induction of nephrogenic systemic fibrosis-like skin lesions in rats. Invest Radiol 2011;46(1):48–56.

30. Ogi S, Fukumitsu N, Tsuchida D, Uchiyama M, Mori Y, Matsui K. Imaging of bilateral striopallidodentate calcinosis. Clin Nucl Med 2002;27(10):721–724.

31. Telgmann L, Sperling M, Karst U. Determination of gadolinium-based MRI contrast agents in biological and environmental samples: a review. Anal Chim Acta 2013;764:1–16.

32. Kanda T, Osawa M, Oba H, et al. High signal intensity in dentate nucleus on unenhanced T1-weighted MR images: association with linear versus macrocyclic gadolinium chelate administration. Radiology doi: 10.1148/radiol.13131669. Published online January 27, 2015. Accessed February 5, 2015.

33. Tweedle MF, Kanal E, Muller R. Considerations in the selection of a new gadolinium-based contrast agent. Appl Radiol 2014.